aerospace

MDPI

Article

Study on the Influence of Soil Parameters on the Cushioning Performance of Landing Airbags

Yichen Wang [1,2], Xuan Zhou [1,2,*], Jingang Liu [1,2,*], Xiaolun Li [1,2], Jiang Wang [1,2] and Pei Zhang [1,2]

[1] School of Mechanical Engineering and Mechanics, Xiangtan University, Xiangtan 411105, China; wyichen24@163.com (Y.W.); lixiaolunn@163.com (X.L.); wangsunnyjiang@outlook.com (J.W.); zhangpei@xtu.edu.cn (P.Z.)

[2] Engineering Research Center of Complex Track Processing Technology & Equipment, Ministry of Education, Xiangtan University, Xiangtan 411105, China

* Correspondence: zhouxuan@xtu.edu.cn (X.Z.); liujingang@xtu.edu.cn (J.L.)

Abstract

To investigate the influence of soil parameters on the cushioning performance of landing airbags, a landing airbag cushioning dynamics model considering soil characteristics was established based on the control volume method and a crushable foam model. Experimental validation was conducted for both the airbag cushioning model and the soil impact model, respectively, with good consistency between simulated and experimental results. Based on the established model, the influence of soil on the cushioning performance of landing airbags was analyzed. The analysis results indicate that soil absorbs energy through compressive deformation during the cushioning process, thereby exhibiting a certain degree of cushioning performance. Softer soil absorbs more energy, and the payload is less prone to rebound. However, excessively soft soil causes the airbag to sink into the soil, hindering the venting of gas outward and resulting in hard landings for payloads. Therefore, three indicators—airbag peak pressure, payload maximum acceleration, and maximum drop height—are used to comprehensively evaluate the cushioning performance of airbags, and the influence laws of soil parameters are quantitatively researched. The research shows that the soil density, shear modulus, and yield parameters A_1 and A_2 significantly influence cushioning performance. Specifically, the shear modulus and yield parameter A_1 exhibit logarithmic growth relationships with the three cushioning performance indicators, while the yield parameter A_2 and soil density show linear growth relationships with the three cushioning performance indicators.

Keywords: airbag; soil; cushioning performance; crushable foam model; orthogonal experiment

Check for updates

Academic Editors: Martin Skote and Craig Lawson

Received: 21 January 2026
Revised: 2 March 2026
Accepted: 9 March 2026
Published: 12 March 2026

Copyright: © 2026 by the authors. Licensee MDPI, Basel, Switzerland. This article is an open access article distributed under the terms and conditions of the Creative Commons Attribution (CC BY) license.

1. Introduction

As highly efficient and reliable cushioning devices, the application of airbags has expanded from the traditional automotive industries to multiple critical fields such as aerospace, national defense and military, logistics, and transportation. In spacecraft recovery, whether for the re-entry capsule of a manned spacecraft or reusable rocket stages, airbags utilize compression deformation and exhaust cushioning to smoothly reduce impact loads to safe levels tolerable by spacecraft structures and internal precise equipment, ensuring a secure landing [1,2]. In defense and military applications, particularly for airdropping heavy equipment [3] and emergency supplies, airbags excel at adapting to complex and variable terrains (such as mountains, sandy areas) and even water surfaces [4], serving as critical buffering devices that ensure smooth landings and immediate operational readiness.

For drone landing cushioning, airbags provide lightweight, reusable landing solutions for fixed-wing or large drones, significantly reducing the risk of structural damage caused by landing environments [5].

Therefore, airbag cushioning technology has become a key technique in the field of cushioning for addressing complex landing conditions due to its outstanding energy absorption efficiency, excellent terrain adaptability, relatively simple structure, and low cost [6]. But current research on cushioning airbags primarily focuses on structural forms [7], geometric parameters, and exhaust control, with little discussion on soil characteristics during experimental design. Nevertheless, due to variations in landing geographical environments, soil properties exhibit significant differences and exert distinct influences on the landing airbag cushioning process [8]. Consequently, the effects of soil must be considered.

Currently, when analyzing the cushioning performance of ground landing airbags, soil is typically simplified as a rigid body [9,10] without considering its effects on the landing airbag cushioning performance. This simplification is reasonable for stiff soil. However, when dealing with soft soil (such as sandy or clay soil) or heavy-load landing conditions, more accurate soil models must be employed. Taylor et al. [11] established a soil model for analyzing the landing cushioning of heavy-load airdrop airbags, but did not specify the exact effects of soil on cushioning performance. Liang and Ji [12] examined how the inter-particle friction coefficient of soil affects the rebound velocity of a re-entry capsule. When the inter-particle friction coefficient is small, the capsule travels a longer distance within the soil, which helps dissipate its kinetic energy, resulting in a lower rebound velocity. Lian et al. [13] analyzed the landing cushioning effects of soil surfaces versus rigid surfaces for heavy-load airdrops. The results show that under crosswind conditions, the maximum vertical overload of airdrop cargo on soil surfaces is approximately 22% lower than on rigid surfaces. Additionally, Gao et al. [14] discovered in cushioning tests for drone recovery airbags that softer ground surfaces yield superior cushioning performance [15]. In summary, soil significantly influences airbag cushioning performance. However, research on how soil parameters affect the performance remains neither systematic nor in-depth.

In response to the above issues, this paper established a dynamic model of airbag cushioning considering soil characteristics, analyzed airbags landing cushioning process under different soils, and researched the influence of soil parameters on the cushioning performance of landing airbags. The research aims to provide valuable insights for the structural design of cushioning airbags, the evaluation of the influence of landing soil on airbag cushioning performance, and the selection of optimal landing sites.

2. Establishment and Validation of Landing Cushioning Models

2.1. Airbag Finite Element Model

There are generally three methods for establishing finite element models of airbags: the control volume (CV) method, the arbitrary Lagrange–Euler (ALE) method, and the smoothed particle hydrodynamics (SPH) method. The ALE method can simulate the unfolding process of folded airbags with greater accuracy. The SPH method is a mesh-free Lagrangian numerical method, particularly suitable for applications involving high-dynamic free-surface flows and complex moving geometries. However, it entails extremely high computational costs, significantly slower speeds compared to the CV and ALE methods, and relatively complex boundary handling. For the airbag cushioning process, the calculation results of the ALE and CV methods are generally consistent, but the CV method offers higher computational efficiency [9,16]. Therefore, the CV method is selected to simulate the airbag cushioning process.

According to the gas state equation,

$$P = (\gamma - 1)\rho e \tag{1}$$

where P is the airbag internal pressure, γ is the specific heat ratio of the gas, ρ is the density of the airbag gas, and e is the specific internal energy of the airbag gas.

Furthermore, the specific heat ratio of the gas γ can be expressed as follows:

$$\gamma = \frac{c_P}{c_V} \tag{2}$$

where c_P is the specific heat capacity at constant pressure, and c_V is the specific heat capacity at constant volume.

And

$$\frac{\mathrm{d}e}{e} = \frac{(1-\gamma)\mathrm{d}V}{V} \tag{3}$$

where V is the airbag gas volume.

By combining Equations (1)–(3), the relationship between airbag pressure P and airbag gas volume V can be obtained.

The control volume method calculates the volume of an airbag by integrating over a surface area as follows:

$$V = \sum_{i=1}^{N} \overline{x_i} n_{ix} A_i \tag{4}$$

where $\overline{x_i}$ is the average value of the x-coordinate of the element node, n_{ix} is the cosine of the angle between the element normal and the x-axis, A_i is the area of the element, and N is the total number of elements in the airbag.

Due to the average flow velocity of the gas inside the airbag being close to zero, the airbag exhaust process can be regarded as the flow process of a standard nozzle. According to the mass flow equation [17], and considering that the velocity of the exhaust gas may reach the speed of sound, the mass flow rate of gas discharged from the airbag can be expressed as follows:

$$\frac{\Delta m}{\Delta t} = C_{\mathrm{or}} A_{\mathrm{or}} P \left(\frac{1}{R_{\mathrm{g}} T}\right)^{\frac{1}{2}} \lambda^{\frac{1}{\gamma}} \left[\frac{2\gamma}{\gamma - 1}\left(1 - \lambda^{\frac{\gamma-1}{\gamma}}\right)\right]^{\frac{1}{2}} \tag{5}$$

where C_{or} is the exhaust port coefficient, A_{or} is the exhaust port area, R_g is the individual gas constant, T is the gas temperature in the airbag, and λ is the ratio of upstream to downstream pressure at the exhaust port.

If $\lambda \geq 0.528$ (subsonic flow), the ratio of upstream to downstream pressure at the exhaust port λ can be obtained as follows:

$$\lambda = \frac{P_{\mathrm{a}}}{P} \tag{6}$$

where P_{a} is the ambient pressure.

If $\lambda < 0.528$ (sonic flow), the ratio of upstream to downstream pressure at the exhaust port λ can be obtained as follows:

$$\lambda = \left(\frac{\gamma + 1}{2}\right)^{\frac{\gamma}{1-\gamma}} \tag{7}$$

Based on the aforementioned modeling approach for the landing airbag cushioning dynamics, the landing process of the cylindrical airbag described in reference [18] was simulated and analyzed using LS-DYNA. In this model, the keyword *AIRBAG_WANG_NEFSKE

was employed to define the airbag behavior. The automatic surface-to-surface contact algorithm (*CONTACT_AUTOMATIC_SURFACE_TO_SURFACE) was used to define the contact interactions, and the keyword *CONSTRAINED_EXTRA_ NODES_SET was utilized to establish the tie constraint between the airbag and the payload. The thickness of the airbag fabric is 0.16 mm, and the fabric is considered an isotropic material with an elastic modulus of 300.0 MPa and a Poisson's ratio of 0.2. The experimental scene from this reference is shown in Figure 1a, and its finite element model is shown in Figure 1b. The parameters of the airbag cushioning dynamics model are listed in Table 1. Since the ground surface in the experiment was an indoor concrete floor, it was simulated using a rigid body. The comparison of the payload acceleration and airbag internal pressure obtained from the finite element model with the experimental results is shown in Figure 2. The simulated results exhibit good consistency with experimental data, with the relative errors for both the airbag maximum internal pressure and the payload maximum acceleration being less than 1.0%. These indicate that the dynamic modeling method for landing airbags is reasonable and feasible.

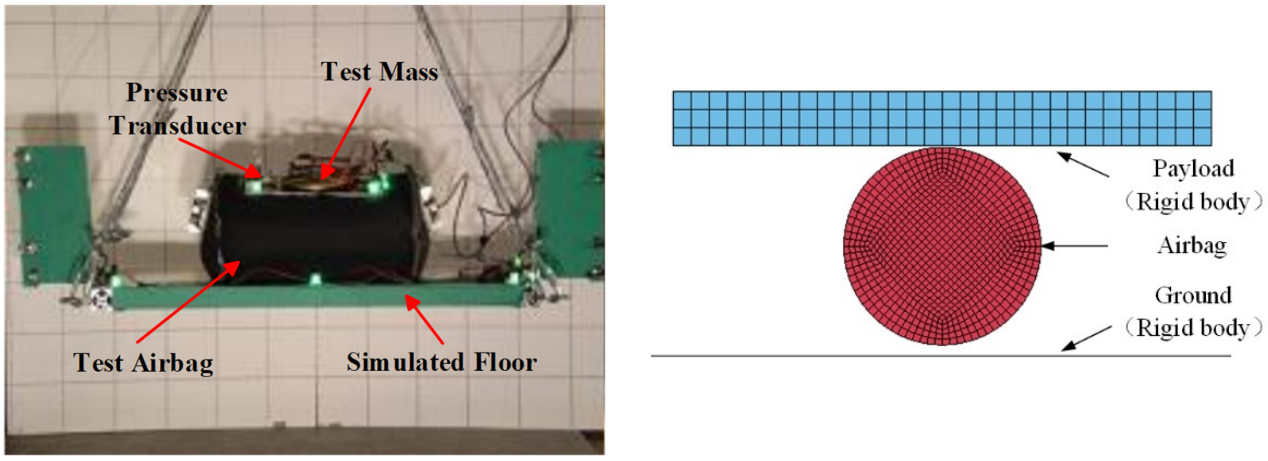


Figure 1. Single airbag drop test. (**a**) Single airbag drop test scene [18]; (**b**) finite element model of single airbag.

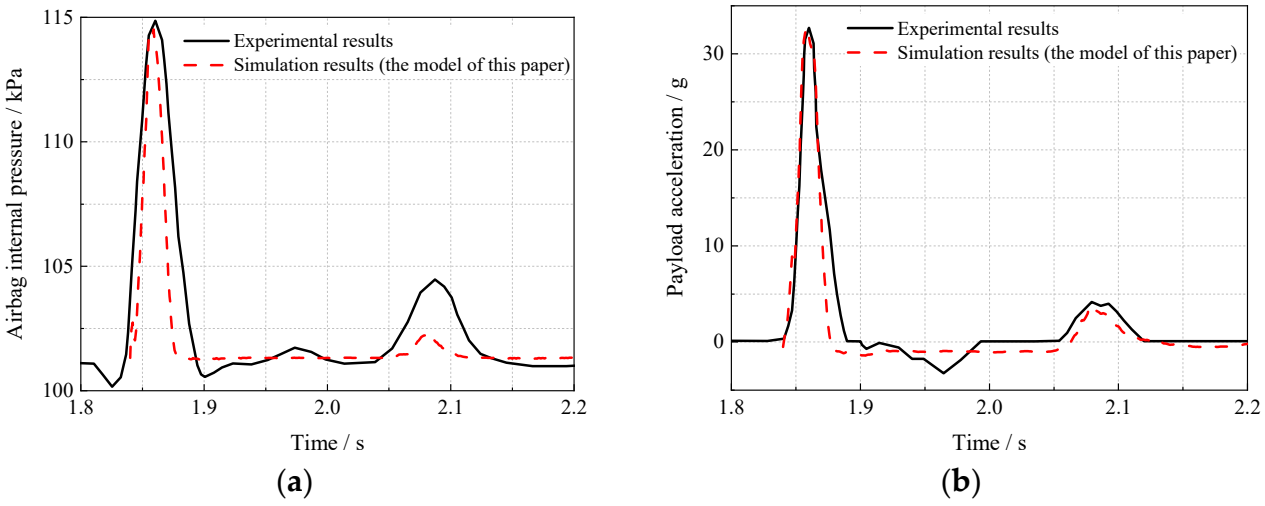


Figure 2. Comparison of simulation results and experimental results for airbag landing cushioning. (**a**) Airbag internal pressure; (**b**) payload acceleration [18].

Table 1. Parameters of the airbag cushioning dynamics model.

Model	Parameter	Symbol	Value	Unit
Airbag	Cross-sectional diameter	D_0	0.22	m
	Busbar length	L_0	0.35	m
	Initial pressure	P_0	101.325	kPa
	Gas temperature	T_0	293.15	K
	Exhaust pressure	P_{op}	114.325	kPa
	Exhaust port area	A_{or}	0.0012	m^2
Payload	Mass	M	2.5	kg
	Initial velocity	v_0	4.8	m/s

Exhaust pressure—P_{op} refers to the exhaust threshold pressure set when the airbag vents.

2.2. Soil Finite Element Model

There are various types of calculation models related to soil, including bilinear models, equivalent linear models, viscoelastic models, ideal elastoplastic models, and crushable models [19]. In scenarios involving soil impact, soft landing cushioning, and re-entry capsule landing, the application of ideal elastoplastic models and crushable models is particularly prevalent [20–22]. The crushable foam model provided by LS-DYNA software has been widely adopted in relevant fields [23]. In the study of aviation structural impact, Fasanella et al. [24] first attempted the MAT_63 crushable foam model, and subsequently developed it into the more comprehensive MAT_005 model, with parameters calibrated through hemispherical penetrometer tests. Kulak and Bojanowski [25] successfully simulated cone penetration tests of sand using MAT_005 and conducted a parameter sensitivity analysis, revealing that density and yield parameters were the most sensitive. Fasanella [26] specifically developed a soil model based on MAT_005 for the Orion spacecraft landing system, calibrating parameters for four different types of soil through triaxial compression, hydrostatic compression, and other test systems. Furthermore, Esmaeili and Tavakoli [27] found that this model could effectively simulate the macroscopic compaction process of saturated sand under explosive loads, and indirectly assess pore pressure effects through settlement analysis. These studies collectively demonstrate that crushable foam models have a broad application foundation and academic recognition in the field of soil impact simulation. This model is also employed for soil modeling in this study.

Due to the brief duration of the landing impact process, the shock wave generated affects a limited area of soil. By calculating the influence range of the shock wave, the required dimensions of the soil model can be determined. In practical calculations, to reduce computational costs, a finite-sized soil model is typically established and subjected to non-reflective boundary conditions to simulate the actual landing surface in an infinite space [22]. The depth of soil affected during the landing impact process can be calculated using the dynamic consolidation method [28] as follows:

$$D = \mu\sqrt{MH} \tag{8}$$

where D is the affected depth; μ is a coefficient related to soil properties, typically ranging from 0.42 to 0.8; M is the mass of the falling object; and H is the free-fall height of the object.

The crushable foam model primarily characterizes soil using parameters such as density ρ, shear modulus G, bulk modulus K, yield function ϕ, and tensile failure cutoff pressure P_c. Among these, the shear modulus under impact can be obtained based on the shear modulus of the dynamic consolidation soil being approximately one-tenth of the small-deformation shear modulus [28] or the shear wave velocity [29]; the bulk modulus can be derived from Poisson's ratio, since soil is essentially incapable of withstanding tensile stress; the tensile failure cutoff pressure can be set to a very small negative value (a

negative value indicates tensile stress); and the yield function ϕ [30] can be expressed using the second stress invariant J_2, hydrostatic pressure P_0, and yield parameters A_0, A_1, and A_2 as follows:

$$\phi = J_2 - [A_0 + A_1 P_0 + A_2 {P_0}^2] \tag{9}$$

In the yield region, the second stress invariant J_2 can be described as

$$J_2 = \frac{1}{3}\sigma_y^2 \tag{10}$$

with

$$\sigma_y = \sqrt{3(A_0 + A_1 P_0 + A_2 {P_0}^2)} \tag{11}$$

Then the second stress invariant J_2 can be expressed as follows:

$$J_2 = A_0 + A_1 P_0 + A_2 {P_0}^2 \tag{12}$$

For the yield parameters A_0, A_1, and A_2, experimental determination is currently not feasible. However, initial estimates can be obtained using the Drucker–Prager model [31], which can be expressed as follows:

$$\sqrt{J_2} + \alpha I_1 - k = 0 \tag{13}$$

with

$$I_1 = \sigma_{ii} = \sigma_1 + \sigma_2 + \sigma_3 = -3P_0 \tag{14}$$

$$\alpha = \frac{\sin\varphi}{\sqrt{3}\sqrt{3 + \sin^2\varphi}} \tag{15}$$

$$k = \frac{\sqrt{3}c\sin\varphi}{\sqrt{3 + \sin^2\varphi}} \tag{16}$$

where φ is the friction angle, and c is the cohesive force.

By combining Equations (13) and (14), the second stress invariant J_2 can be expressed as follows:

$$J_2 = k^2 + 6\alpha k P_0 + 9\alpha^2 {P_0}^2 \tag{17}$$

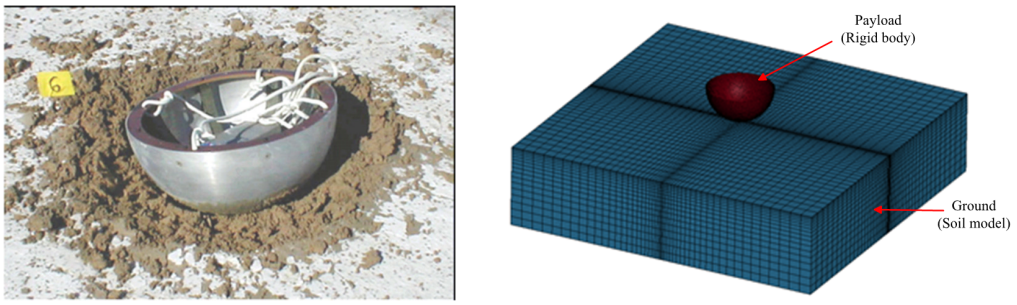
By comparing Equations (12) and (17), the yield parameters A_0, A_1, and A_2 can be described as follows:

$$\begin{cases} A_0 = k^2 \\ A_1 = 6\alpha k \\ A_2 = 9\alpha^2 \end{cases} \tag{18}$$

Based on the variation range of soil physical and mechanical parameters, the theoretical value ranges for each parameter in the model can be obtained through the above calculations.

The low-speed soil impact experiment in reference [32] was simulated; the experimental scene from this reference is shown in Figure 3a, and the finite element model is shown in Figure 3b. The falling object is a hollow hemisphere with a mass of 12.05 kg, defined as a rigid body. The soil model dimensions are as specified in 0.5 m × 1.0 m × 1.0 m [29], with the soil bottom fixed. The soil type is stiff soil, with its characteristic parameters as shown in Table 2 [29,32]. The yield parameters A_0, A_1, and A_2 can be obtained by Equation (18). The touchdown velocities of the iron balls are 35.0 m/s and 44.9 m/s, respectively. The comparison between simulated and experimental results is shown in Figure 4. It can be observed that the two sets of data agree well, with the maximum acceleration error being

less than 3.0% in both cases, validating the effectiveness of the established model. Therefore, when establishing a landing airbag cushioning dynamic model that accounts for soil properties, a crushable foam model can be employed to represent the soil.

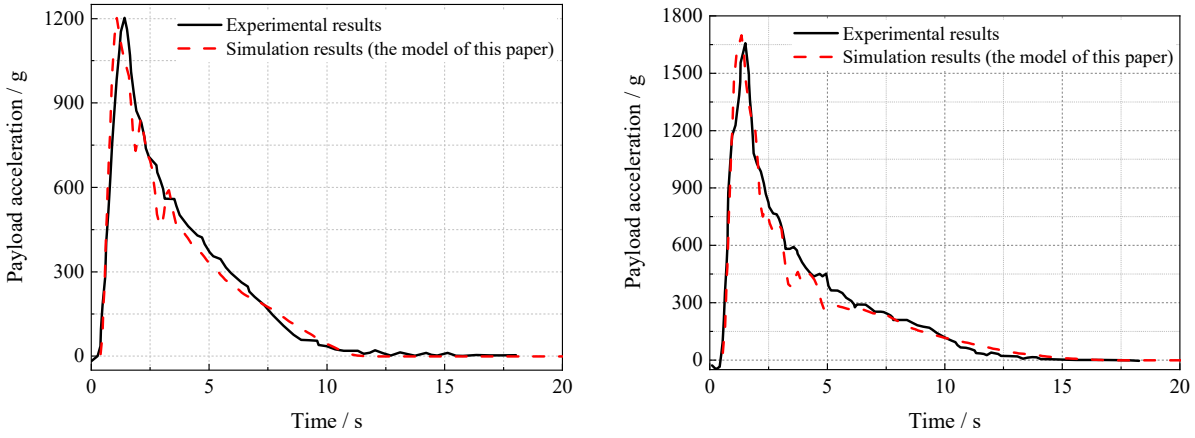


(**a**) (**b**)

Figure 3. Low-speed soil impact test. (**a**) Hemisphere impact test scene [32]; (**b**) finite element model of hemisphere impact test.

Table 2. Characteristic parameters of stiff soil [29,32].

ρ/(kg/m^3)	G/MPa	K/MPa	A_0/Pa^2	A_1/Pa	A_2	P_c/Pa
1453.84	1.840	68.948	0.307	0.389	0.123	-6.90×10^{-8}



(**a**) (**b**)

Figure 4. Comparison of experimental and simulation results for soil impact. (**a**) Touchdown velocity of falling object: 35.0 m/s; (**b**) touchdown velocity of falling object: 44.9 m/s [32].

3. Analysis of Landing Airbag Cushioning Process Considering Soil Properties

Based on the modeling method for airbags and soil described in Section 2, a finite element model of the landing airbag cushioning dynamics is constructed, taking soil properties into account. The airbag structural parameters are listed in Table 1, with a touchdown velocity of 4.8 m/s. According to Equation (8), the affected soil depth can be calculated as 0.057 to 0.108 m. Considering the differences among various soil types, the dimensions of the soil model are appropriately scaled up, ultimately setting the soil model size to 0.5 m $\times$ 1.5 m $\times$ 1.5 m. The finite element model of airbag cushioning dynamics is shown in Figure 5.

When establishing soil models using crushable foam models, two soil types are selected for analysis: one is stiff soil with characteristic parameters as shown in Table 2, the other is soft soil (the soft soil refers to mudflats or sandy areas) with characteristic parameters as shown in Table 3. The comparison of the internal pressure, payload acceleration,

velocity, and displacement of the landing airbag considering soil characteristics during the cushioning process with the calculated results of the soil rigid body model is shown in Figure 6. These results indicate that regardless of whether the soil model is based on a crushable foam model or assumed as a rigid body, the landing airbag system experiences rebound and secondary impact. However, softer soil results in a smaller rebound height and a greater drop height for the payload. Consequently, soil deformation has a significant influence on the cushioning process of landing airbags, with softer soil exerting a greater effect.

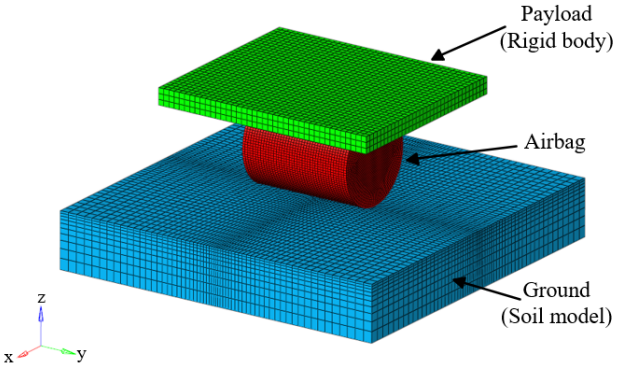


Figure 5. Finite element model of landing airbag cushioning dynamics considering soil properties.

Table 3. Characteristic parameters of sandy soil.

ρ/(kg/m^3)	G/MPa	K/MPa	A_0/Pa^2	A_1/Pa	A_2	P_c/Pa
1453.84	1.840	68.948	0	0	0.3	0

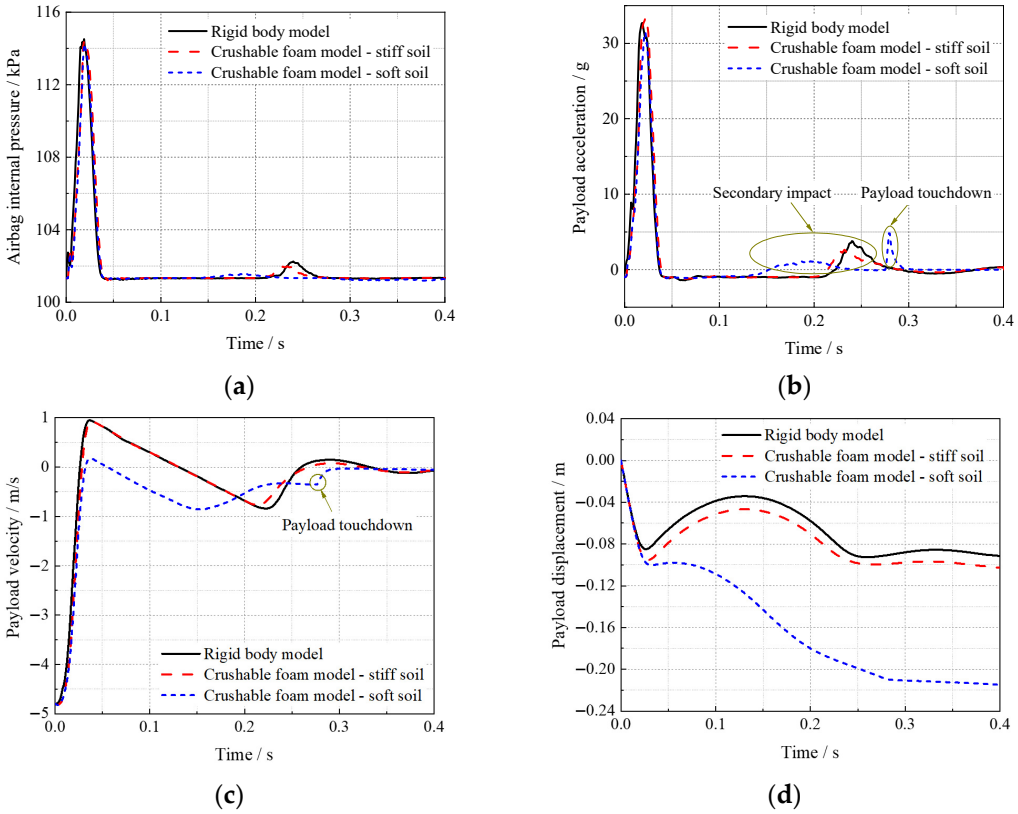


Figure 6. Comparison of calculated results between the soil rigid body model and the crushable foam model. (**a**) Airbag internal pressure; (**b**) payload acceleration; (**c**) payload velocity; (**d**) payload displacement.

The airbag peak pressure, payload maximum acceleration, and maximum drop height under different soil conditions are shown in Table 4. We can observe that the airbag peak pressure decreases progressively across the three soil types, though the differences are minor. This is primarily because the stiffness of the airbag is lower than that of the soil. When the airbag internal pressure reaches its maximum, the soil deformation is very small (for soft soil, the peak internal pressure is reached at 0.019 s, at which the maximum vertical displacement at the center point of the soil is only 0.0018 m). The crushable foam model accounts for soil deformation, resulting in a slightly larger contact area between the airbag and the ground compared to the rigid body model. Consequently, the peak acceleration of the payload also increases. Additionally, the softer the soil, the greater the payload drop height. This occurs because the softer soil exhibits progressively larger deformations during cushioning. At 0.4 s. Figure 7 shows the deformation of two types of soil in the z-direction, with maximum deformations of 0.014 m and 0.158 m, respectively. For stiff soil, the compression zone approximates a rectangle; for soft soil, it approximates an ellipse. When the soil is soft, excessive deformation causes the airbag to sink completely into the soil (as shown in Figure 8), resulting in the payload directly impacting the ground, as depicted in Figure 6b.

Table 4. Calculated results of different soil types.

Soil Type	Peak Pressure P_{max}/kPa	Maximum Acceleration a_{max}/g	Maximum Drop Height h_{max}/m
Rigid body	114.52	34.08	0.093
Stiff soil	114.41	33.43	0.103
Soft soil	114.24	31.40	0.215

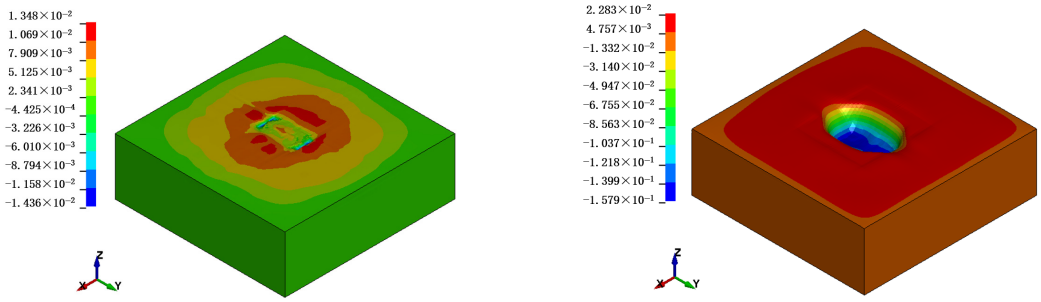


Figure 7. Deformation of two types of soil in the z-direction. (**a**) Stiff soil; (**b**) soft soil.

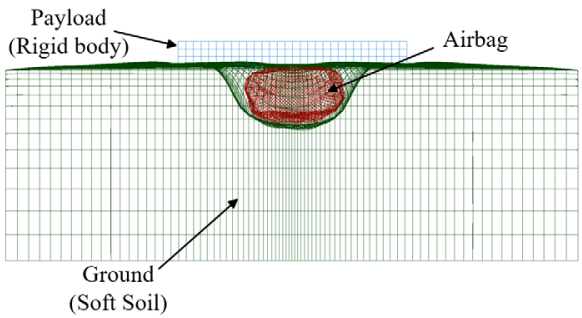


Figure 8. State of the airbag system for the soft soil model at 0.4 s.

In summary, during the cushioning process, the soil absorbs energy through compressive deformation, and the softer the soil, the greater the deformation energy (as shown in Figure 9). Therefore, the greater the payload maximum displacement at first falling (as

shown in Figure 6d), and the smaller the payload total energy after rebound (as shown in Figure 9), the smaller the maximum height of rebound and the greater the maximum drop height. These demonstrate that the soil possesses a certain cushioning capacity. If the ground is stiff soil, it can be simplified as a rigid body; if it is soft soil, its deformation must be considered. When the soil is sufficiently soft, the airbag system will not rebound but a hard landing will occur. It is evident that soil parameters significantly influence the landing cushioning process of the airbag, necessitating research into the laws of their influence.

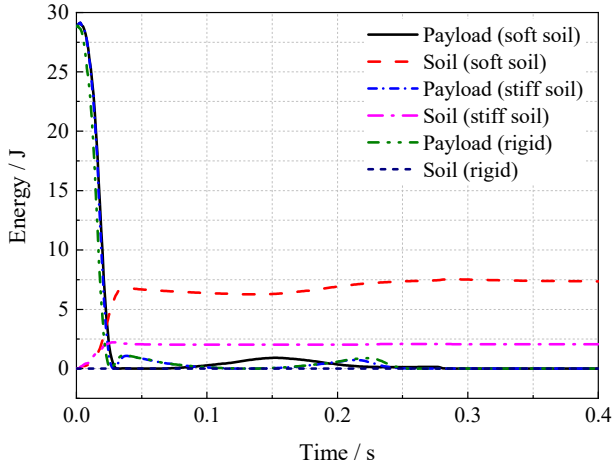


Figure 9. Energy of the payload and soil during the cushioning process.

It should be specifically noted that in the aforementioned simulation study on airbags, the area of the exhaust port was assumed to remain constant even when the airbag sank into soil.

4. Influence of Soil Parameters on Airbag Cushioning Performance

Generally speaking, the payload maximum acceleration and the airbag maximum internal pressure during the airbag landing process are the two most critical indicators for evaluating airbag cushioning performance. The former is used to evaluate whether supplies or equipment are normally available after landing, while the latter is used to evaluate whether the airbag fabric has ruptured. Additionally, the airbag should not sink into the soil. As shown in the analysis in Section 3, when the airbag sinks into the soil, it may cause the payload to directly impact the ground and also hinder the airbag's outward deflation. Obviously, the softer the soil, the deeper the airbag sinks, which corresponds to a greater maximum drop height of the payload and a higher risk during the landing cushioning process. Therefore, it is necessary to consider the payload's maximum drop height as an important evaluation indicator. The maximum drop height is defined as the absolute value of the payload's maximum displacement from the moment the airbag contacts the soil until the end of the cushioning process. In summary, to quantitatively analyze the influence of soil parameters on the cushioning performance of landing airbags, three parameters, namely the payload maximum acceleration, the airbag maximum internal pressure, and the payload maximum drop height, are identified as evaluation indicators for landing cushioning performance.

The six main parameters describing the crushable foam model include soil density ρ; shear modulus G; bulk modulus K; and yield parameters A_0, A_1, and A_2. The actual soil is complex, but mainly related to these six parameters. By analyzing the influence of these parameters on airbag cushioning performance, the influence of different soils on airbag cushioning performance can be obtained.

4.1. Sensitivity Analysis of Soil Parameters

Sensitivity analysis [33] of soil parameters can identify the primary soil parameters affecting the cushioning performance of landing airbags [26]. Firstly, an orthogonal experiment with six factors and four levels was designed, namely L_{32} (4^6), with the values for each factor shown in Table 5, yielding a total of 32 experimental groups.

Table 5. The factors and values of orthogonal experimental design.

Parameter	Value Range	Orthogonal Experimental Design Value	Description
$\rho/(\mathrm{kg/m^3})$	1000.0~2500.0	1000.0, 1500.0, 2000.0, 2500	
G/MPa	0.1~50.0	0.1, 1.0, 10.0, 50.0	
K/MPa	1.0~170.0	1.0, 10.0, 100.0, 150.0	Source: Reference [26].
$A_0/\mathrm{kPa^2}$	0~535.0	0, 10.0, 100.0, 500.0	
A_1/kPa	0~105.0	0, 1.0, 10.0, 100.0	
A_2	0~0.75	0.1, 0.3, 0.5, 0.7	Source: Equation (18).

Subsequently, simulation analysis was conducted by using a finite element model of landing airbag cushioning dynamics that accounts for soil properties. The numerical simulation results are presented in Table 6.

Table 6. Results of orthogonal experimental design.

No.	P_{max}/kPa	a_{max}/g	h_{max}/m	No.	P_{max}/kPa	a_{max}/g	h_{max}/m
1	114.32	30.86	0.213	17	114.63	32.58	0.145
2	114.17	31.54	0.120	18	114.27	32.84	0.112
3	114.30	33.23	0.113	19	114.29	31.55	0.116
4	114.61	33.05	0.115	20	114.27	29.96	0.116
5	114.26	30.88	0.220	21	114.35	32.38	0.171
6	114.13	29.98	0.214	22	114.40	33.31	0.133
7	114.28	34.02	0.104	23	114.07	31.70	0.114
8	114.12	32.10	0.112	24	114.52	33.09	0.106
9	114.28	31.93	0.111	25	114.32	31.64	0.141
10	114.22	32.90	0.108	26	114.57	32.31	0.108
11	114.16	32.37	0.116	27	114.49	33.44	0.111
12	114.20	32.70	0.131	28	114.54	33.70	0.111
13	114.40	31.35	0.116	29	114.17	31.72	0.141
14	114.45	33.34	0.125	30	114.25	31.92	0.167
15	114.02	31.23	0.102	31	114.51	32.24	0.109
16	114.28	32.18	0.102	32	114.19	31.32	0.104

Finally, based on the previously designed L_{32} (4^6) orthogonal experiment with six factors and four levels, along with 32 groups of simulation results, a range analysis [34] was performed on these data to obtain the extent of influence for each parameter. K_{jk} is the sum of the responses of experimental groups whose factor serial number is j ($j \leq 6$) and level serial number is k ($k \leq 4$), and $\overline{K_{jk}}$ is the average of K_{jk}, which is called the index value. The difference between the maximum value and the minimum value of the index values is defined as the range of experimental groups whose factor serial number is j. That is,

$$R_j = \max(\overline{K_{j1}}, \overline{K_{j2}}, \cdots, \overline{K_{j4}}) - \min(\overline{K_{j1}}, \overline{K_{j2}}, \cdots, \overline{K_{j4}}) \quad (19)$$

R_j reflects the fluctuation of the response when the level serial number is changed for the experimental groups whose factor serial number is j. Therefore, the larger the R_j, the greater the impact of this factor on the response, and the more important it is. In addition,

the influence degree P_{R_j} of the factor whose serial number is j on the response can be obtained by normalization as follows:

$$P_{R_j} = \frac{R_j}{\sum_{i=1}^{6} |R_i|} \times 100\% \tag{20}$$

Therefore, by comparing the magnitude of the range R_j (or the influence degree P_{R_j}) of each design parameter, the main parameters influencing the response can be obtained. Moreover, the positive and negative influences can be obtained according to the positive and negative differences between the two levels corresponding to the range. The positive influence indicates that the larger the value of the factor, the larger the response value, and the negative effect is just the opposite.

The sensitivity analysis results for various soil parameters on the cushioning performance of the airbag, obtained using the range analysis method, are shown in Figure 10. It can be observed that the primary influencing parameters for the airbag peak pressure are the shear modulus G and soil density ρ, both exhibiting positive effects. That is, the larger these two parameters, the greater the peak pressure. The main factors affecting the payload maximum acceleration are soil shear modulus G and yield parameter A_2, both exhibiting positive effects. The primary influencing parameters for the payload maximum drop height are yield parameter A_1 and soil density ρ, both exhibiting negative effects. That is, as these two parameters increase, the maximum drop height decreases. Overall, the shear modulus G, yield parameters A_1 and A_2, and soil density ρ significantly influence the cushioning performance of landing airbags, with their influence degree decreasing in that order. The following sections will investigate the specific influence of these four parameters.

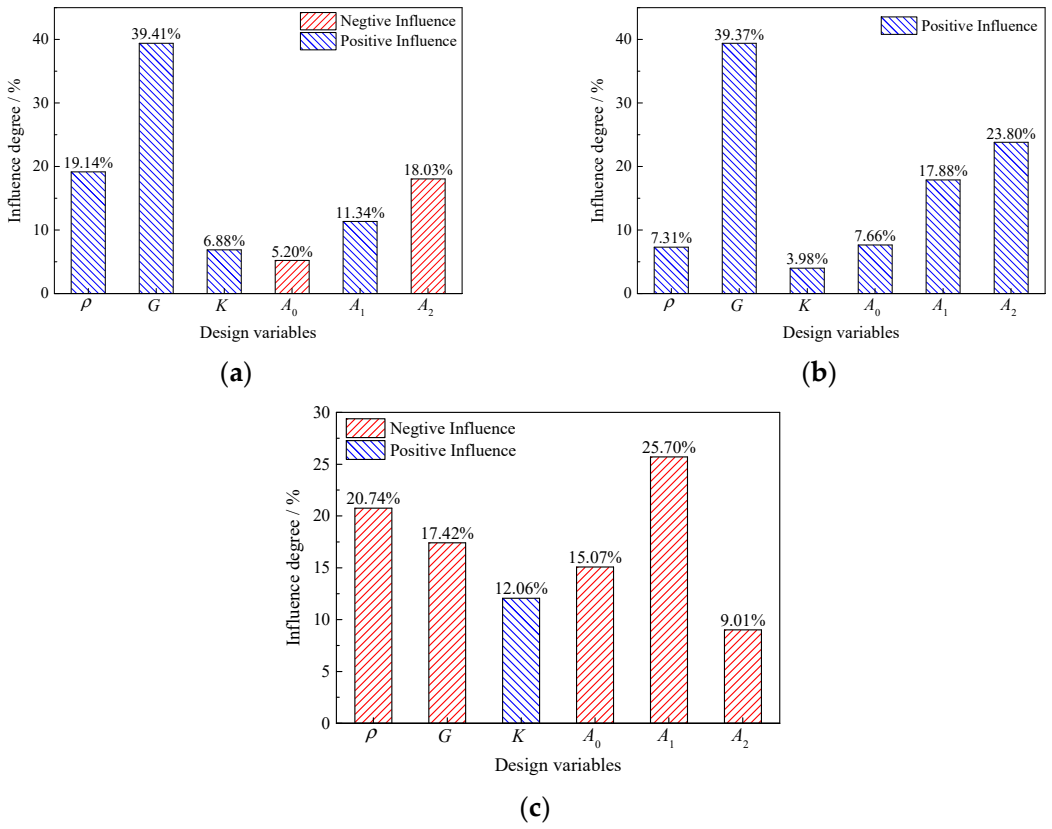


Figure 10. Sensitivity analysis results for various soil parameters. (**a**) Peak pressure; (**b**) maximum acceleration; (**c**) maximum drop height.

4.2. Analysis of Variance

To evaluate the statistical significance of the impact of various factors, an analysis of variance was conducted on the results of the orthogonal experiment. The analysis results are presented in Tables 7–9. It can be observed that for peak pressure, density ρ, shear modulus G, and yield parameter A_2 have an extremely significant impact ($p < 0.01$), while yield parameter A_1 has a significant impact ($p < 0.05$). For maximum acceleration, shear modulus G and yield parameter A_2 have an extremely significant impact ($p < 0.01$), and yield parameter A_1 has a significant impact ($p < 0.05$). For maximum drop height, density ρ, shear modulus G, and yield parameter A_1 have an extremely significant impact ($p < 0.01$), while yield parameter A_0 has a significant impact ($p < 0.05$). This result is consistent with the range analysis (Figure 10), providing a statistical basis for the importance of factors and enhancing the reliability of the conclusions.

Table 7. Analysis of variance for peak pressure.

Source of Variance	Sum of Squares	Degrees of Freedom	Mean Square	*F* Value	*p* Value
ρ	0.223	3	0.074	7.40	0.004 **
G	0.381	3	0.127	12.70	<0.0001 **
K	0.018	3	0.006	0.60	0.625
A_0	0.008	3	0.003	0.30	0.825
A_1	0.112	3	0.037	3.70	0.039 *
A_2	0.540	3	0.180	18.00	<0.0001 **

Note: $R^2 = 0.908$, * represents significant ($p < 0.05$), ** represents extremely significant ($p < 0.01$).

Table 8. Analysis of variance for maximum acceleration.

Source of Variance	Sum of Squares	Degrees of Freedom	Mean Square	*F* Value	*p* Value
ρ	1.469	3	0.490	1.40	0.287
G	16.284	3	5.428	15.51	<0.0001 **
K	1.322	3	0.441	1.26	0.329
A_0	1.345	3	0.448	1.28	0.322
A_1	3.821	3	1.274	3.64	0.041 *
A_2	17.545	3	5.848	16.71	<0.0001 **

Note: $R^2 = 0.905$, * represents significant ($p < 0.05$), ** represents extremely significant ($p < 0.01$).

Table 9. Analysis of variance for maximum drop height.

Source of Variance	Sum of Squares	Degrees of Freedom	Mean Square	*F* Value	*p* Value
ρ	9.140	3	3.047	13.85	<0.0001 **
G	4.570	3	1.523	6.92	0.005 **
K	0.757	3	0.252	1.15	0.363
A_0	3.040	3	1.013	4.60	0.020 *
A_1	15.230	3	5.077	23.08	<0.0001 **
A_2	1.520	3	0.507	2.30	0.125

Note: $R^2 = 0.923$, * represents significant ($p < 0.05$), ** represents extremely significant ($p < 0.01$).

4.3. Interaction Assessment

To clarify the coupling effect between key soil parameters (density ρ, shear modulus G, yield parameters A_1, A_2) on the cushioning performance indicators of airbags, based on the results of orthogonal experiments, the strength and regularity of the interaction between each parameter were analyzed to determine whether the interaction is a secondary factor

affecting the cushioning performance. The analysis results indicate that the interaction between various soil parameters is weaker than the single-factor main effect, and the effects on the peak pressure of the airbag, the maximum acceleration of the payload, and the maximum drop height are all secondary. The specific rules are as follows:

For the peak pressure of the airbag, the interaction between the shear modulus G and soil density ρ is relatively significant ($\bar{I} = 0.124$), and the two exhibit a synergistic enhancement effect, as shown in Table 10. Namely, when G and ρ increase simultaneously, the increase in peak pressure is slightly greater than the sum of single-factor effects, which indicates that the high stiffness and high density of soil jointly lead to a more rapid rise in the airbag internal pressure during the impact process. However, the interaction between yield parameters A_1 and A_2 is the weakest ($\bar{I} = 0.021$).

Table 10. Average interaction intensity of soil parameters on airbag peak pressure.

Parameter Pair	ρ-G	ρ-A_1	ρ-A_2	G-A_1	G-A_2	A_1-A_2
Average interaction intensity $\bar{I}$ (kPa)	0.124	0.046	0.078	0.052	0.097	0.021

For the maximum acceleration of the payload, the dominant interaction is between the shear modulus G and yield parameter A_2 ($\bar{I} = 0.356$), with a significant synergistic effect, as shown in Table 11. This is because the shear modulus G determines the soil's resistance to shear deformation, and A_2 controls the yield characteristics of the soil; their joint action intensifies the rigid response of the soil to the airbag impact, thus increasing the impact load on the payload. The interactions between other parameter pairs are relatively weak ($\bar{I} < 0.15$), and no obvious synergistic or antagonistic effects are observed.

Table 11. Average interaction intensity of soil parameters on payload maximum acceleration.

Parameter Pair	ρ-G	ρ-A_1	ρ-A_2	G-A_1	G-A_2	A_1-A_2
Average interaction intensity $\bar{I}$ (g)	0.128	0.085	0.142	0.093	0.356	0.067

For the maximum drop height, the most prominent interaction is between the yield parameter A_1 and soil density ρ ($\bar{I} = 0.018$), showing a weak antagonistic effect: the decrease in maximum drop height caused by the simultaneous increase in A_1 and ρ is slightly smaller than the superposition of their single-factor effects. All other parameter pairs show extremely weak interactions ($\bar{I} < 0.01$), as shown in Table 12, which indicates that the influence of each parameter on the maximum drop height is basically independent, and the coupling effect can be neglected in engineering analysis.

Table 12. Average interaction intensity of soil parameters on payload maximum drop height.

Parameter Pair	ρ-G	ρ-A_1	ρ-A_2	G-A_1	G-A_2	A_1-A_2
Average interaction intensity $\bar{I}$ (m)	0.009	0.018	0.007	0.006	0.008	0.005

4.4. Research on Influence Laws of Key Soil Parameters

The key parameters affecting airbag cushioning performance have been determined through sensitivity analysis, but the specific influence laws of these parameters are still unclear. Next, we will investigate four parameters separately: shear modulus G, yield parameters A_1 and A_2, and soil density ρ. Moreover, to analyze the influence of different landing loads, two sets of analysis working conditions with different payload masses have

been added. The calculation results are shown in Table 13, in which the soil model is a rigid body model. It is not difficult to find that as the payload mass increases, the peak pressure and maximum drop height increase, while the payload maximum acceleration decreases.

Table 13. Airbag landing cushioning performance at different payload masses when the soil is a rigid body.

Payload Mass M/kg	Peak Pressure P_m/kPa	Maximum Acceleration a_{max}/g	Maximum Drop Height h_{min}/m
2.5	114.52	32.70	0.093
12.5	133.42	22.28	0.166
25.0	157.22	21.21	0.187

4.5. Shear Modulus G

The cushioning performance of landing airbags under different soil shear moduli G is shown in Figure 11, where the shear modulus is taken as 0.1 MPa, 0.5 MPa, 1.0 MPa, 5.0 MPa, 10.0 MPa, and 50.0 MPa. It can be observed that the peak pressure and maximum acceleration increase with rising shear modulus, while the maximum drop height decreases with increasing shear modulus, which is consistent with the sensitivity analysis results of soil parameters. Furthermore, a logarithmic growth relationship exists between the shear modulus G and all three cushioning performance indicators. When G $\geq$ 10 MPa, the peak pressure, maximum acceleration, and maximum drop height remain essentially unchanged.

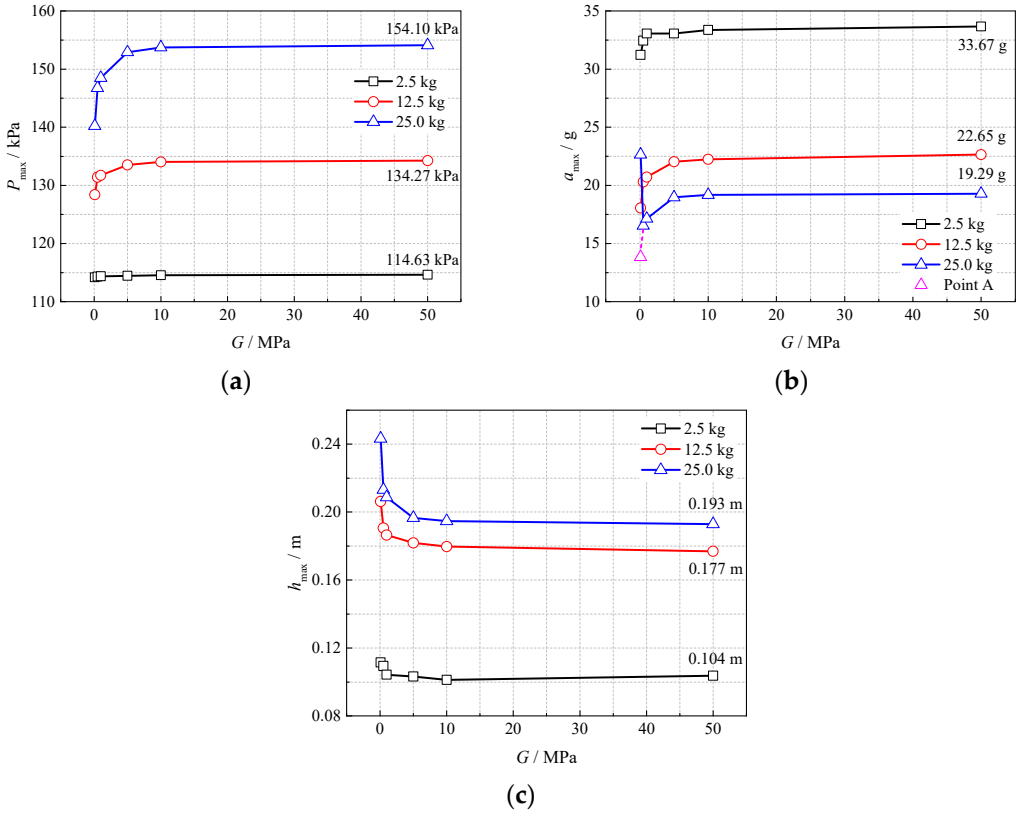


Figure 11. Landing airbag cushioning performance under different shear moduli *G*. (**a**) Peak pressure; (**b**) maximum acceleration; (**c**) maximum drop height.

It should be specifically noted that for the working condition of M = 25.0 kg, when the shear modulus G is 0.1 MPa, the excessively soft soil causes the payload to collide directly with the ground, resulting in a maximum acceleration of 22.63 g. If the payload's hard landing is disregarded, the maximum acceleration during the cushioning process

reaches 13.84 g, as shown at Point A in Figure 11b, which still complies with the above-mentioned laws.

4.5.1. Yield Parameter A_1

Six different values of yield parameter A_1 (0.0 kPa, 1.0 kPa, 5.0 kPa, 10.0 kPa, 50.0 kPa, 100.0 kPa) were selected for analysis. The cushioning performance of the landing airbag is shown in Figure 12. It is evident that as the yield parameter A_1 increases, both the peak pressure and maximum acceleration continue to rise, while the maximum drop height decreases accordingly. Similarly, yield parameter A_1 exhibits a logarithmic growth relationship with all three cushioning performance indicators. When $A_1 \geq 10$ kPa, the peak pressure, maximum acceleration, and maximum drop height tend toward constant values.

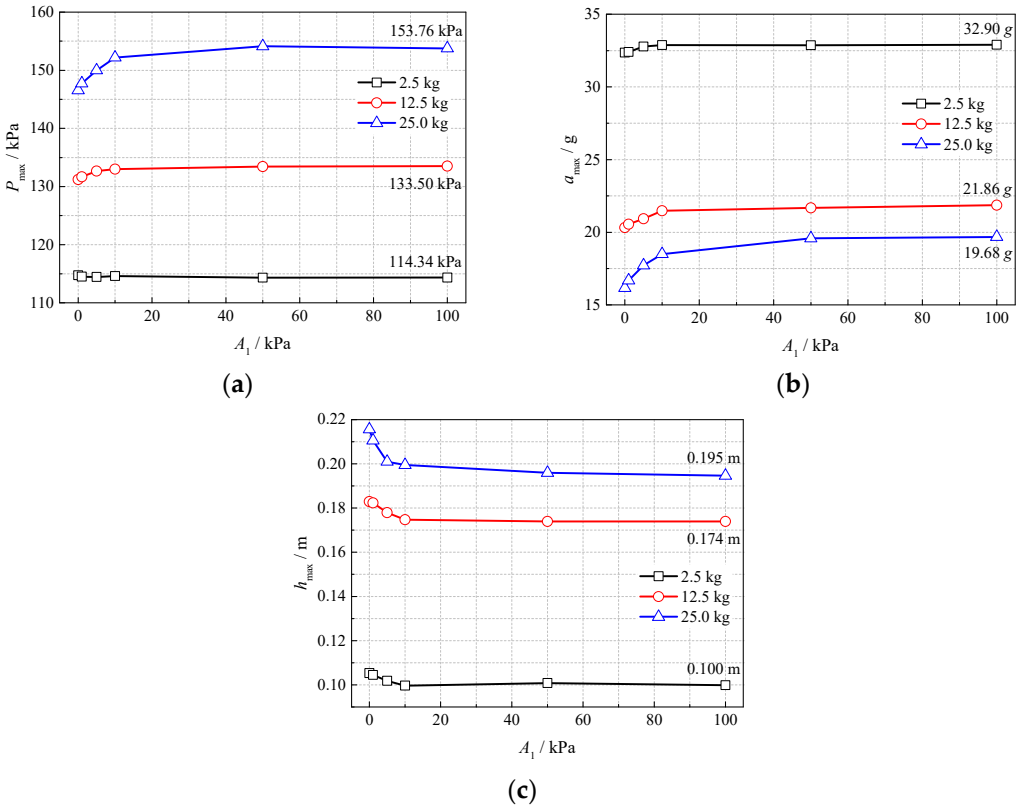


Figure 12. Landing airbag cushioning performance under different yield parameters A_1. (**a**) Peak pressure; (**b**) maximum acceleration; (**c**) maximum drop height.

4.5.2. Yield Parameter A_2

The cushioning performance of landing airbags with different values of yield parameter A_2 is shown in Figure 13. We can observe that as the yield parameter A_2 increases, both the peak pressure and maximum acceleration increase, while the maximum drop height decreases. In addition, yield parameter A_2 exhibits an approximate linear growth relationship with all three cushioning performance indicators.

4.5.3. Soil Density ρ

Different soil densities were analyzed, ranging from 500.0 to 3000.0 kg/m^3. The cushioning performance of the landing airbag is depicted in Figure 14. It is obvious that the peak pressure and maximum acceleration increase with soil density, while the maximum drop height decreases accordingly. Likewise, soil density exhibits an approximate linear growth relationship with all three cushioning performance indicators.

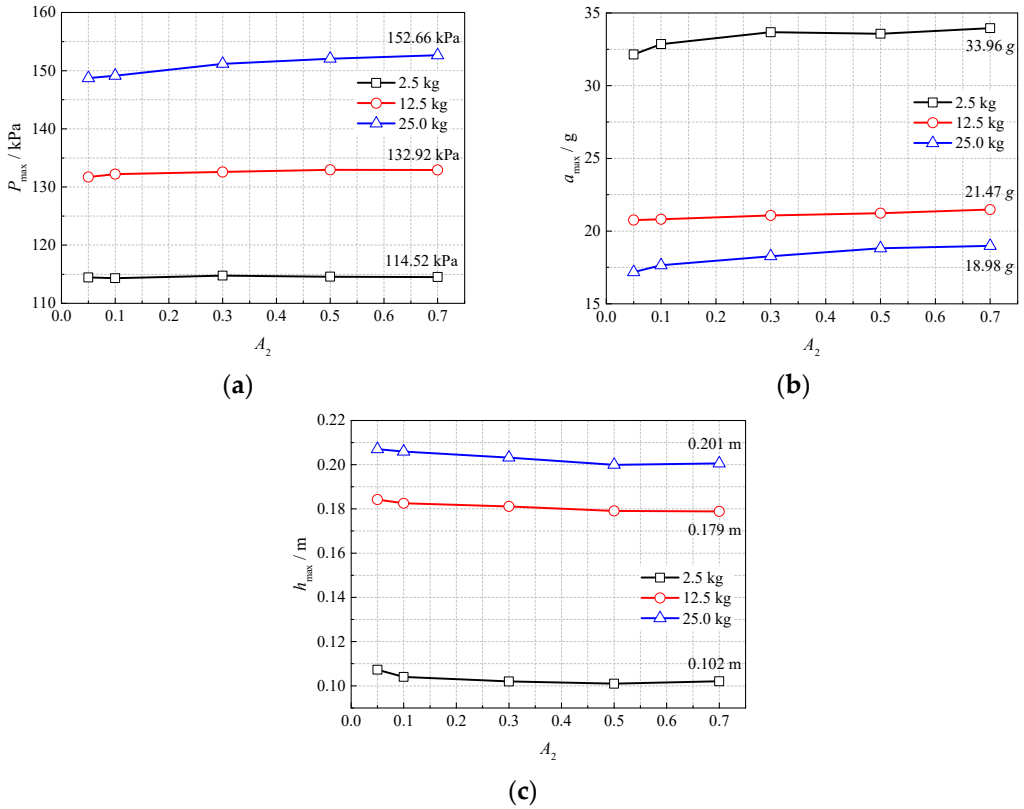


Figure 13. Landing airbag cushioning performance under different yield parameters A_2. (**a**) Peak pressure; (**b**) maximum acceleration; (**c**) maximum drop height.

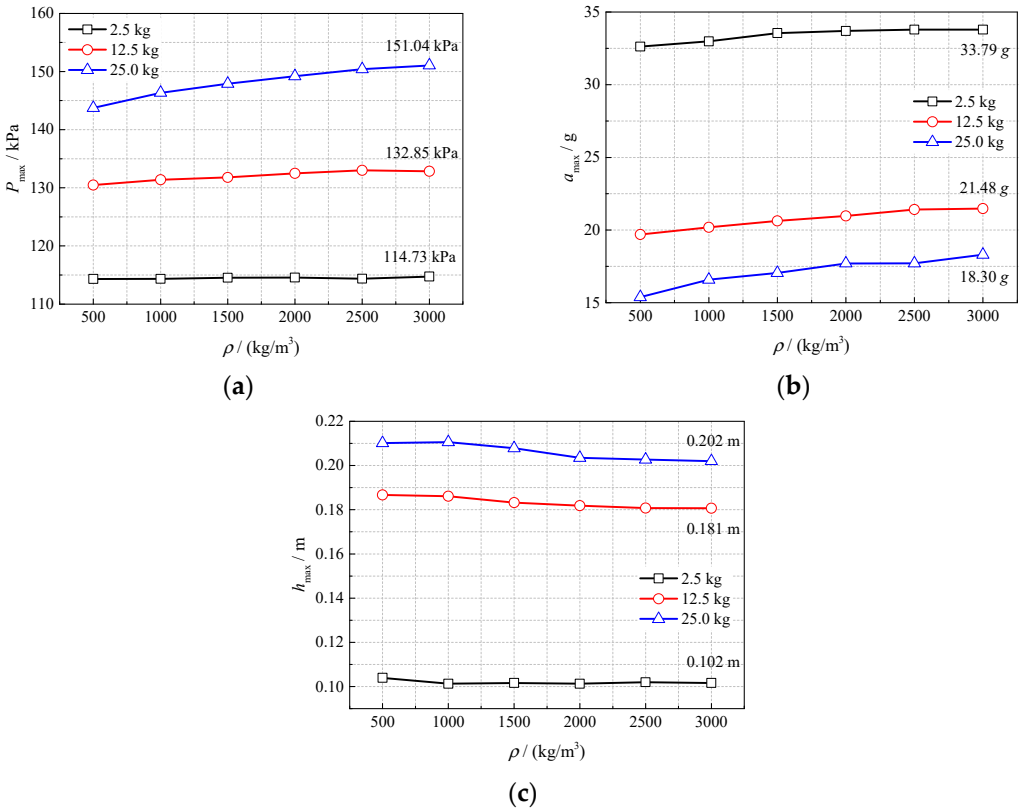


Figure 14. Landing airbag cushioning performance under different soil densities ρ. (**a**) Peak pressure; (**b**) maximum acceleration; (**c**) maximum drop height.

On the other hand, for the four parameters of soil density ρ, shear modulus G, and yield parameters A_1 and A_2, the above influence laws remain consistent under different landing loads. Moreover, the greater the payload mass, the more pronounced the corresponding laws become. In other words, the above laws only manifest when the soil undergoes a certain degree of deformation. If the airbag cushioning system cannot crush the soil, it can be simplified as a rigid body.

Notably, with the increase in soil parameters (density ρ, shear modulus G, and yield parameters A_1 and A_2), when the payload mass is 2.5 kg and 12.5 kg, the peak pressure, payload maximum acceleration, and maximum drop height all approach the results when the soil is a rigid body. However, when the payload mass is 25.0 kg, compared to calculation results assuming soil as a rigid body, the peak pressure is reduced by 3.12~6.18 kPa, and the payload maximum acceleration decreases by 1.53~2.91 g. These results indicate that when the payload mass reaches 25.0 kg, soil deformation becomes significant and must be considered. At this point, simplifying it as a rigid body is no longer applicable.

Essentially, whether soil will be crushed is not only related to soil characteristic parameters but also to the pressure it is subjected to. Regardless of landing working conditions, once the soil is subjected to excessive pressure, it will influence the landing cushioning process of the airbags. However, parameters such as the cushioning airbag size, payload mass, and initial velocity all influence the pressure that the soil is subjected to. Therefore, if the landing site has been selected, the pressure on the soil can be reduced by adjusting parameters such as airbag size, inflation pressure, exhaust port size, payload mass, and landing velocity, thereby avoiding the airbag sinking into the soil.

5. Conclusions

Airbag cushioning systems are widely applied in spacecraft recovery, heavy airdrops, and unmanned aerial vehicle soft landings. Among these applications, soil significantly influences the landing cushioning process of airbags. This paper established a finite element model for landing airbag cushioning dynamics considering soil characteristics based on the CV method and a soil foam model, and investigated the influence of soil parameters on airbag cushioning performance. The main conclusions are as follows:

1. During the cushioning process, soil absorbs energy through compressive deformation, resulting in a reduction in the total energy of the payload after rebound and a decrease in rebound height. These demonstrate that soil also has a certain degree of cushioning performance. Furthermore, the softer the soil, the greater the deformation, and the greater the payload maximum drop height. However, from a reliable perspective, excessively soft soil should be avoided when selecting landing sites. Because it may cause the airbag to sink into the soil, the exhaust port may be partially blocked by the soil, resulting in a decrease in effective exhaust area and hindering venting gas outward, thereby affecting the buffering performance. The payload may even directly impact the ground. Moreover, transporting and moving the payload on soft soil is also difficult.
2. Three cushioning performance indicators—airbag peak pressure, payload maximum acceleration, and maximum drop height—were defined. By making a horizontal contrast of these indicators, a suitable landing site soil can be determined. Sensitivity analysis of soil parameters was conducted on six parameters of the soil foam model. The analysis results indicate that four parameters—soil density ρ, shear modulus G, and yield parameters A_1 and A_2—exert a significant influence on the above three indicators. Therefore, these parameters should be focused on investigation and analysis when selecting landing sites.

3. Further research reveals that the airbag peak pressure and payload maximum acceleration increase with the rise in the above four key soil parameters, while the payload maximum drop height decreases accordingly. Among these, the soil shear modulus G and yield parameter A_1 exhibit logarithmic growth relationships with the three cushioning performance indicators, while the yield parameter A_2 and soil density ρ show linear growth relationships with the three cushioning performance indicators. The greater the payload mass, the more pronounced these laws become. Based on these laws, the specific changes in cushioning performance can be obtained when soil parameters vary.

6. Declaration of Applicable Boundaries

The crushable foam model (*MAT_SOIL_AND_FOAM) adopted in this paper is suitable for research scenarios focusing on macroscopic responses (such as peak pressure, maximum acceleration, and maximum drop height). It can be used for simulation analysis of fully drained conditions, low-saturation soil, or sandy soil media that are insensitive to pore pressure effects. However, it cannot describe the generation and evolution of pore water pressure, the volume–shear coupling effect, and significant strain rate effects. Therefore, it is not suitable for impact problems in saturated soft soil or under undrained conditions. For complex problems beyond the aforementioned scope of application that require a detailed characterization of pore pressure evolution or high-strain-rate mechanical behavior, it is recommended to adopt more-advanced soil constitutive models, such as the Drucker–Prager Cap model, the Mohr–Coulomb cap model, or the *MAT_FHWA_SOIL model in LS-DYNA. These models can more comprehensively reflect the true mechanical behavior of soil under impact loading.

Author Contributions: Writing—original draft, investigation, methodology, and formal analysis, Y.W.; writing—review and editing, funding acquisition, validation, and project administration, X.Z.; writing—review and editing, funding acquisition, supervision, and project administration, J.L.; investigation and software, X.L.; formal analysis and data curation, J.W.; project administration and resources, P.Z. All authors have read and agreed to the published version of the manuscript.

Funding: The work in this paper was supported by the Hunan Provincial Natural Science Foundation of China (Grant No. 2025JJ80215), Hunan Provincial Major Science and Technology Research Project (Grant No. 2025QK2005), Hunan Province Key Research and Development Program Provincial and Municipal Joint Project (Grant No. 2024QY2009), Hunan Provincial Administration for Market Regulation Science and Technology Program Project (Grant No. 2024KJJH23), and Xiangtan University Doctoral Research Start-Up Project (Grant No. 2023113101509).

Data Availability Statement: The data is contained within the article.

Conflicts of Interest: The authors declare no conflicts of interest.

References

1. Bown, N.; Darley, M. Advanced airbag landing systems for planetary landers. In Proceedings of the 18th AIAA Aerodynamic Decelerator Systems Technology Conference and Seminar, Munich, Germany, 23–26 May 2005; p. 1615.
2. Shen, X.Y.; Wang, X.F.; Liu, C.S. A review of the airbag landing system for spacecraft. *Chin. J. Aeronaut.* **2025**, *38*, 103569. [CrossRef]
3. Zhao, Q.; Wang, H.; Lu, C. Design and analysis of a cushioning airbag system for heavy airdropped equipment in High-Altitude environments. *Aerospace* **2025**, *12*, 768. [CrossRef]
4. Li, L.; Chen, J.; Ma, Y. A study on the lateral static stability of a helicopter floating on water with a flexible airbag. *Aerospace* **2025**, *12*, 664. [CrossRef]

5. Cui, B.; Zhang, Y.; Dong, H. Test and numerical analysis for water entry of elastic cabin from amphibious aircraft. *Aerosp. Sci. Technol.* **2024**, *150*, 109168. [CrossRef]
6. Tutt, B.; Sandy, C.; Corliss, J. Status of the development of an airbag landing system for the Orion crew module. In Proceedings of the 20th AIAA Aerodynamic Decelerator Systems Technology Conference and Seminar, Seattle, WA, USA, 4–7 May 2009; p. 2923.
7. Zhou, X.; Zhou, S.M.; Li, D.K. Direct folding method of cylindrical airbag and its application in landing buffer. *J. Aerosp. Eng.* **2022**, *35*, 04022083. [CrossRef]
8. Watanabe, K.; Horiguchi, T.; Tanaka, K. Effect of soil type on running performance of small lunar rover. *Aerospace* **2025**, *12*, 24. [CrossRef]
9. Fu, X.H. Analysis on characteristics of structural impact response of airborne armored vehicle in landing process. *IOP Conf. Ser. Mater. Sci. Eng.* **2019**, *484*, 012024. [CrossRef]
10. Li, J.; Wang, H.; Rui, Q. Research on cumulative damage assessment method for airborne vehicle at landing based on finite element analysis. *J. Syst. Simul.* **2014**, *26*, 208–214.
11. Taylor, A.; Benney, R.; Bagdonovich, B. Investigation of the application of airbag technology to provide a soft-landing capability for military heavy airdrop. In Proceedings of the 16th AIAA Aerodynamic Decelerator Systems Technology Conference and Seminar, Boston, MA, USA, 21–24 May 2001; p. 2045.
12. Liang, S.; Ji, S. DEM-FEM coupling analysis of safe landing of reentry capsule considering landing attitude and rebound response. *J. Aerosp. Eng.* **2021**, *34*, 04021035. [CrossRef]
13. Lian, W.X.; Hou, B.; Sun, J.H. Numerical analysis of landing cushioning process for heavy-load airdropped airbags on different ground conditions. *Adv. Aeronaut. Sci. Eng.* **2022**, *13*, 68–75.
14. Gao, H.H.; Wang, H.H.; Zhang, H.Y. Experimental study on the cushioning performance of a recovery airbag for a certain type of unmanned aerial vehicle. *Spectr. Recovery Remote Sens.* **2021**, *42*, 30–38.
15. Mou, H.; Wang, Z.; Xie, J. Comprehensive crashworthiness simulation analysis of a large aircraft fuselage barrel section in various crash scenarios. *Aerosp. Sci. Technol.* **2024**, *152*, 109338. [CrossRef]
16. Zhou, X.; Zhou, S.M.; Li, D.K. Research on design and cushioning performance of combined lunar landing airbag. *Acta. Astronaut.* **2022**, *191*, 55–78.
17. Cole, J.K.; Waye, D.E. *BAG: A Code for Predicting the Performance of a Gas Bag Impact Attenuation System for the PATHFINDER Lander*; Sandia National Laboratories: Albuquerque, NM, USA, 1993.
18. Sydney, D. An Airbag-Based Crew Impact Attenuation System for the Orion Crew Exploration Vehicle. Doctoral Dissertation, Massachusetts Institute of Technology, Cambridge, MA, USA, 2011.
19. Xie, D.Y. *Soil Dynamics*; Higher Education Press: Beijing, China, 2011.
20. Fasanella, E.L.; Jackson, K.E.; Kellas, S. Soft soil impact testing and simulation of aerospace structures. In Proceedings of the 10th International LS-DYNA Users Conference, Dearborn, MI, USA, 8–10 June 2008.
21. Kim, Y.B.; Jeong, H.J.; Park, S.M. Prediction and validation of landing stability of a lunar lander by a classification map based on touchdown landing dynamics' simulation considering soft ground. *Aerospace* **2021**, *8*, 380. [CrossRef]
22. Zhang, D.P.; Lei, Y.J.; Duan, J.B. Influence analysis of soil parameters on the landing impact characteristics of the return capsule. *J. Vib. Shock.* **2014**, *33*, 120–125.
23. Fasanella, E.L. Multi-terrain Earth landing systems applicable for manned space capsules. *J. Aerosp. Eng.* **2009**, *22*, 201–213.
24. Fasanella, E.L. *Developing Soil Models for Dynamic Impact Simulations*; NASA Langley Research Center: Hampton, VA, USA, 2009.
25. Kulak, R.F.; Bojanowski, C. Modeling of Cone Penetration Test Using SPH and MM-ALE Approaches. In Proceedings of the 8th European LS-DYNA Users Conference, Strasbourg, France, 23–24 May 2011.
26. Fasanella, E.L.; Heymsfield, E.; Hardy, R.C. Assessment of Soil Modeling Capability for Orion Contingency Land Landing. *J. Aerosp. Eng.* **2010**, *25*, 125–131.
27. Esmaeili, M.; Tavakoli, B. Finite element method simulation of explosive compaction in saturated loose sandy soils. *Soil Dyn. Earthq. Eng.* **2019**, *116*, 446–459. [CrossRef]
28. Du, H.L. *Improved Calculation and Analysis of Landing Impact Cushioning System for Spacecraft Return Capsule Under Abnormal Conditions*; Tsinghua University: Beijing, China, 2003.
29. Yan, J.; Yang, L.; Zhang, Z.J. Validation study of lunar soil mechanics material model. In Proceedings of the 2009 National Symposium on Structural Dynamics, Orlando, FA, USA, 9–12 February 2009; pp. 111–116.
30. Klasztorny, M.; Nycz, D.B.; Dziewulski, P. Numerical modelling of post-ground subsystem in road safety barrier crash tests. *Eng. Trans.* **2019**, *67*, 513–534.
31. Drucker, D.C.; Prager, W. Soil mechanics and plastic analysis or limit design. *Q. Appl. Math.* **1952**, *10*, 157–165. [CrossRef]
32. Fasanella, E.; Jones, Y.; Knight, N. Low-velocity Earth-penetration test and analysis. In Proceedings of the 19th AIAA Applied Aerodynamics Conference, Anaheim, CA, USA, 11–14 June 2001; p. 1388.

33. Quinn, D.; Colbert, S.; Nolan, D.C. Propulsion system integration on truss-braced aircraft: Structural performance sensitivity to architectural design parameters. *Aerosp. Sci. Technol.* **2025**, *159*, 109987. [CrossRef]
34. Zhou, X.; Zhou, S.M.; Li, D.K. Optimal design of airbag landing system without rebound. *IOP Conf. Ser. Mater. Sci. Eng.* **2019**, *531*, 012001. [CrossRef]

Disclaimer/Publisher's Note: The statements, opinions and data contained in all publications are solely those of the individual author(s) and contributor(s) and not of MDPI and/or the editor(s). MDPI and/or the editor(s) disclaim responsibility for any injury to people or property resulting from any ideas, methods, instructions or products referred to in the content.